Integrating UAS photogrammetry and Digital Image Correlation for high-resolution monitoring of large landslides

Francesco Mugnai[1]*, Andrea Masiero [1]

[1]   Department of Civil and Environmental Engineering, University of Florence, via di S.Marta, 3 - 50139 Firenze, Italy; francesco.mugnai@unifi.it

*   Correspondence: francesco.mugnai@unifi.it

Abstract: This paper shows the results of applying high-resolution Unmanned Aircraft System (UAS) photogrammetric surveying on a large landslide. A real case study, where permanently installing GCPs could be complex, where natural shaped and formed land pose severe limitations in deploying ground targets with optimal geometric configuration. We analysed performances in terms of survey accuracy obtained by performing photogrammetric surveys through the Zenmuse P1 DJI optical camera and Phantom 4 Pro 2. In combination with DJI Matrice 300 UAS, the P1 camera allows direct georeferencing through GNSS observations in RTK mode. Photogrammetric surveys, performed through different georeferencing methods, have been compared. Several targets have been permanently installed on the ground over the maximum vegetation height to guarantee long-lasting reference over the years in the area, which is characterised by a diffuse short vegetation coverage. Multitemporal UAS surveys have been then compared using Digital Image Correlation (DIC) algorithms, and deformation maps have been produced. Afterwards, DIC results were compared with observations made by the GNSS ground-based permanent receivers resulting in a standard deviation of 0,077 m. Through results analysis, good accordance between ground-based GNSS observations and DIC analysis on the photogrammetric surveys have been identified for the same time span. To conclude, this type of landslide presents a moderate deformation speed; in such a case, effective deformations monitoring could be achieved using pseudo-direct georeferencing, which permitted a 0.24 m accuracy on the whole tested area.

Keywords: Digital Image Correlation (DIC), Unmanned Aerial System (UAS), GNSS; deformation map; monitoring

1. Introduction

Performing UAS photogrammetric surveying for landslide monitoring is an emerging methodology that well fit both the need to have periodic surveys and the capability to reach secluded areas [1]–[4]. One of the most deployed remote sensing techniques for landslide monitoring has undoubtedly been RADAR SAR Interferometry [5]–[9]. Its flexibility, together with long-range, accuracy and wide field of view, posed RADAR technology, both airborne [10], [11] and ground-based [12]–[14], as a reference in landslide monitoring. With such a technique, building a map of deformations representative of a wide area and maintaining a range resolution of 10-3 m, even from kilometric distances. However, hi-cost is limiting access to the RARAD technology. More often, good results have been obtained through the integrated use of different techniques [15]–[17]. Handling such a monitoring system could be difficult for minor stakeholders. In this fold, the photogrammetry technique has become increasingly used in this criticality. For technical reasons, performing UAS photogrammetric survey allows for discontinuous temporal monitoring only, even in the case of tethered aircraft, which could guarantee a longer-lasting flying [18], [19]. Nevertheless, considering many landslides have a slow or moderate velocity [20], a monitoring revisiting period of some hours or days could be considered an excellent way to monitor deformative patterns efficiently.

Some steps must be performed following a specific workflow to properly carry out a photogrammetric survey and obtain a consistent 3D topographic reconstruction. The in-field activities must be followed by specific processing. Post-processing is usually carried out in some hours/days, often using an office workstation, due to the considerable number of pictures to be elaborated for a photogrammetric reconstruction. For this reason, the time span to obtain a photogrammetric reconstruction could be considered as a daily recurrence. Depending on the landslide size, the landslide velocity, and the element at risk, a photogrammetric campaign could be considered an effective tool to create a topographic survey of the landslide body. A monitoring campaign could be performed by a diachronic comparison between two or more topographic surveys. By applying the Interferometric RADAR technique, a deformation map of the viewed area can be easily obtained. This seems far from a photogrammetric survey that produces a topographic model of the viewed area after photogrammetric reconstruction. Usually, indirect georeferencing is applied to the photogrammetric reconstruction process to obtain good accuracy that can be consistently applied to a deformative process like a landslide. Obtaining a centimetric accuracy on a photogrammetric survey could be considered a feasible objective if a good camera, a sound Ground Control Point (GCP) networks are arranged, and a proper flight altitude and camera settings have been chosen. Even air stability, which can interact with three canopy or long grass, can influence the quality of the final topographic model. However, once a georeferenced topographic model has been produced within a given accuracy, it can be compared with another georeferenced topographic model of the same area taken with a photogrammetric survey made at a different time. After creating DEMs from the 3d topographic models, a Dem of Difference (DoD) could be realised to investigate volumes changes and profile variations [21]–[23]. However, a pixel-based approach is to be considered to generate a deformation map of the studied area. Digital Image Correlation (DIC) technique [24], [25] can be applied. During the last decades, DIC has been applied for various engineering purposes.

The wide range of scales and the adequate accuracy and resolution that DIC can guarantee make it a very versatile technique. It is indeed used for architectural and structures deformations [26], tensile stress on construction materials [27], restoration [28], from microscale [29] to large scale applications [30]. This method allows specific algorithms to recognise light intensity patterns corresponding to the reflected light from the undeformed and deformed object configurations. In this way, deformations of small subsets of the image, thereby the deformations of small subsets of the actual object surface, can be measured [31], [32]. DIC is usually performed on multitemporal images of the same scene [33]. A Landslide, as long as a picture of the same area and with a similar point of view to each other, is used, could be considered a heterogeneous reflective body and investigated with the DIC technique [34].

Some researchers applied DIC on ortomosaics elaborated from photogrammetric surveys [35]–[37] to obtain a deformation map of the landslide area, and good results have been obtained.

In order to foster some advancements, some new features have been added to the research line in this work. In particular, a large area of investigation has been selected, direct and indirect georeferencing has been performed for the photogrammetric reconstruction process; the GCP and Check Point (CKP) networks has been linked to the local GNSS permanent monitoring system. A 45 Mpx camera has been used to guarantee hi-resolution pictures, maintaining a small Ground Sampling Distance, which, considering the considerable size of the surveyed landslide, allowed to maintain a good flying altitude and reduce the time of the survey. The small GSD also allows for obtaining an effective orthophoto mosaic resolution.

Camera settings as aperture, shutter speed, magnification, and iso have been determined to optimise the UAS survey considering the landslide's size and velocity. The expected primary outcome is a deformation map of the landslide. For a specific deformative process, an effective monitoring system is expected to perceive displacements and resolutions that sufficiently characterise the process. Using a low time resolution monitoring

system to monitor a fast landslide could not be effective, and adopting a low spatial resolution to perceive small particle movements.

The Calita landslide, the investigated area, hosts a well-studied landslide. Several studies have been performed, and different monitoring systems have been installed during the last 20 years. Thanks to these previous studies, the velocity range is accurately known; the photogrammetric surveys carried out in this research have been tailored to fit the velocity of the monitored process, i.e. surveys time recurrence, GSD, orthophoto mosaic resolution.

Furthermore, a GNSS network has been observing the landslide movements for the last five years; its outcomes have been used as a reference control for the performed survey.

The presented research activity has been designed to give convenient indications to implement effective landslide deformation monitoring using UAS photogrammetry. Survey and analysis were carried out on a real case study, where permanently installing GCPs could be economically tricky for local or regional administrations and where natural shaped and formed land poses severe limitations in deploying ground targets with optimal geometric configuration.

1.1. Study area

The Ca'Lita landslide, which is inside the administrative boundary of Baiso and into Reggio Emilia Province (Italy), was chosen as the study area for this research (Figure 1). The landslide is in the Secchia River Valley and is located in the Nord-Est mountainside of the northern Apennines [38]. Ca'Lita has a longitudinal length of approximately 3 km and a maximum width of about 1.4 km [39]. It is a large compound landslide composed of a roto-translational rockslide in the head zone, with flysch rock masses, and in the downslope has a translational earth slide-earthflow acting clayey complexes and debris material from the degradation of flysch rock masses [40].

The landslide of Ca'Lita has a long succession of reactivations that have threatened the safety of infrastructures and people in the crowning and valley area. In April 2004, an initial paroxysmal reactivation caused significant retrogression and advancement of the landslide [34].
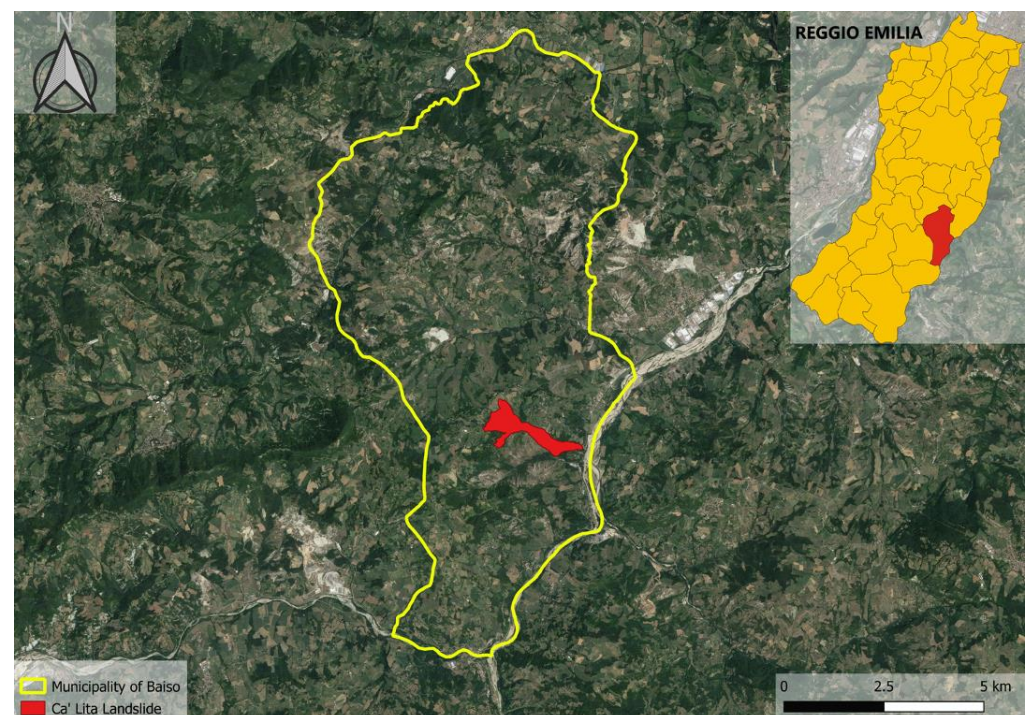
Figure 1. Aerial view of the Study area.

2. Materials and Methods

The presented work executed photogrammetric surveys performed applying different georeferencing methods. In the study area, which is characterised by a diffuse short vegetation coverage, several targets have been permanently installed on the ground, over the maximum vegetation height, to guarantee a lasting reference on the ground over the years. Subsequently, photogrammetric flight missions were performed using nadiral and inclined camera angles of view. The installed Ground targets, used as GCPs and CkPs, were measured with GNSS observations in RTK and NRTK mode, both with a permanent local base station and a Virtual Local Station. Then the picture datasets were processed through photogrammetric software. The photogrammetric reconstruction processes were carried out using three different georeferencing methods. "A" method consists of a pseudo-direct georeferencing, in which coordinates of camera positions were directly provided by the onboard UAS GNSS receiver in RTK mode and then processed through SfM software. "B" method consists of an indirect georeferencing procedure, in which GCPs and CkPs coordinates have been observed through GNSS in field survey with a receiver in RTK mode. Through "C" method GCPs coordinates have been observed through GNSS in field survey with a receiver in RTK mode; furthermore, camera positions were directly provided by the onboard UAS GNSS receiver in RTK mode and then processed through SfM software.

The accuracy obtained through the A, B, C modes were investigated for three selected areas: the upper part of the landslide, so-called "Piana", the central part of the landslide, so-called "Colata", and the whole landslide area.
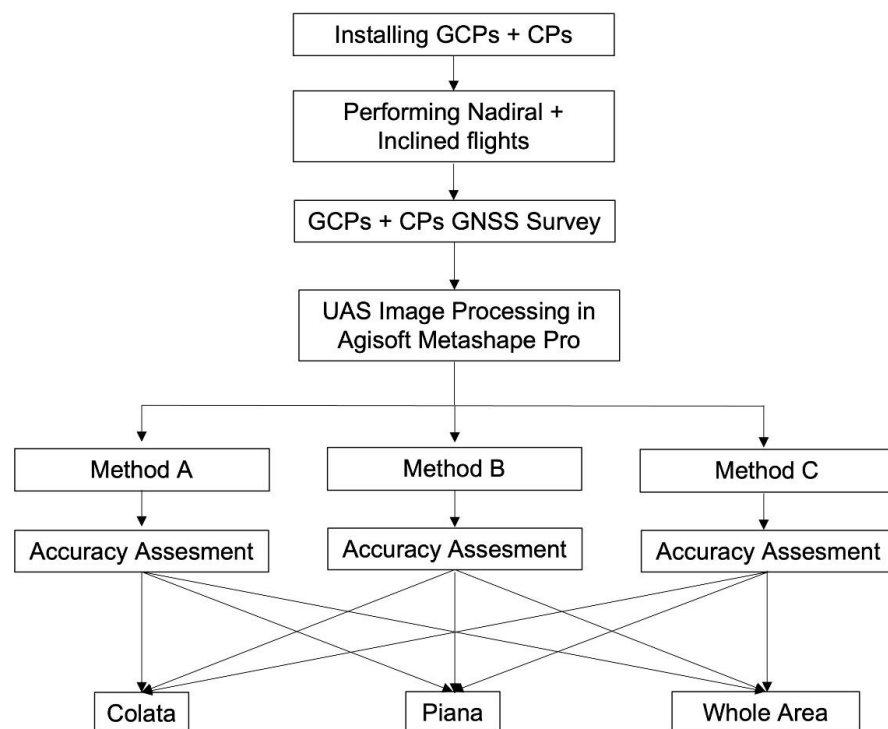
Figure 2. Workflow of the activities.

Processing multitemporal UAS surveys were finally compared using Digital Image Correlation (DIC) algorithms and deformation maps have been produced. Afterwards, DIC results were compared with observations made by the GNSS ground based permanent receivers. A diachronic comparison of surveys produced in October 2020 and April 2021 was also performed and compared with observations made by the permanent GNSS monitoring system.
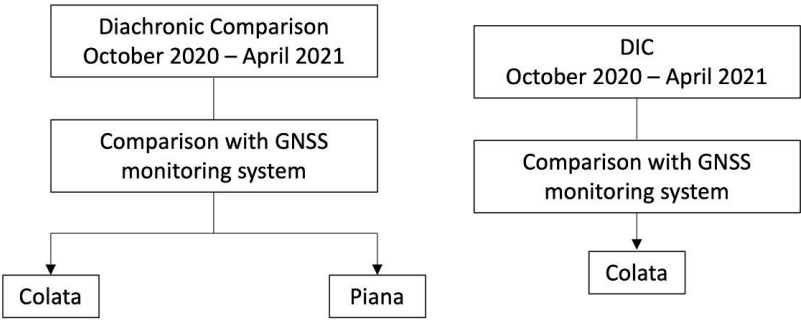
Figure 1. Diachronic comparisons (left) and DIC analysis (right) workflows.

2.1. Photogrammetric surveys

Through photogrammetric surveys, orthomosaics have been generated using SfM Metashape software. Performing two photogrammetric campaigns and then producing orthomosaics at different times allows for comparing, identifying differences, and monitoring surface deformations. Monitoring Ca'Lita landslide outperformed two photogrammetric campaigns at two different times, considering these phenomena' high spatial and temporal variability.

2.1.1. UAS and Cameras

During photogrammetric surveys, two different drones and cameras were used. In October 2020, the DJI Phantom 4, a commercial-grade multi-copter drone with an integrated   optical   camera (DJI, 2016). DJI Matrice 300 RTK has been used for the April 2021 survey. It is an industrial aircraft equipped with RTK technology for a centimetre position (Dilectro, 2020). It integrates a 45MP full-frame sensor within the Zenmuse P1 camera, a global mechanical shutter, and an interchangeable fixed-focus DJI dl lens in a three-axis stabilised gimbal (DJI, 2020). Tables 1 and 2 below compare the equipment used.

Table 1. UAS characteristics.

UAS		
Characteristics	**DJI Phantom 4**	DJI Matrice 300 RTK
Maximum takeoff weight	1.39 kg	9.00 kg
Flight range	30 min	55 min
Transmission distance	7.00 km	15.00 km
Maximum speed of ascent	6.00 m/s	6.00 m/s
Maximum speed of descent	3.00 m/s	7.00 m/s
Maximum horizontal speed	13.80 m/s	17.00 m/s

Table 2. Camera characteristics.

CAMERA		
Characteristics	**DJI Phantom 4 optical**	Zenmuse P1
Sensor	CMOS 1"	Full Freame
Pixel	20 MP	45 MP
Lens	FOV 84.00° 8.80 mm/24 mm	FOV 63.50° 35 mm
Shutter speed	1/2000 sec	1/2000 sec
ISO range	100 - 3200 (automatic) 100- 12800 (manual)	100 - 25600
Range aperture	f/2.8 - f/11	f/2.8 – f/16
Minimum shutter range	2.00 sec	0.70 sec

2.1.2. Aerial Image acquisition

An automatic flight mode programmed through UgCS Software (Engineering, 2019) (Figure 1) has been used in October and April survey campaigns. UgCS permits to set the specifications of drones and cameras in addition to Ground Sample Distance (GSD), side and forward overlap and camera tilt. Using planned flights allows to maintain speed, overlapping, and GSD reasonably constant along with the same photogrammetric campaign, and guarantees reliable repeatability for the various campaigns at different times, even months or years later. The characteristics of the flights are shown in Table 3.
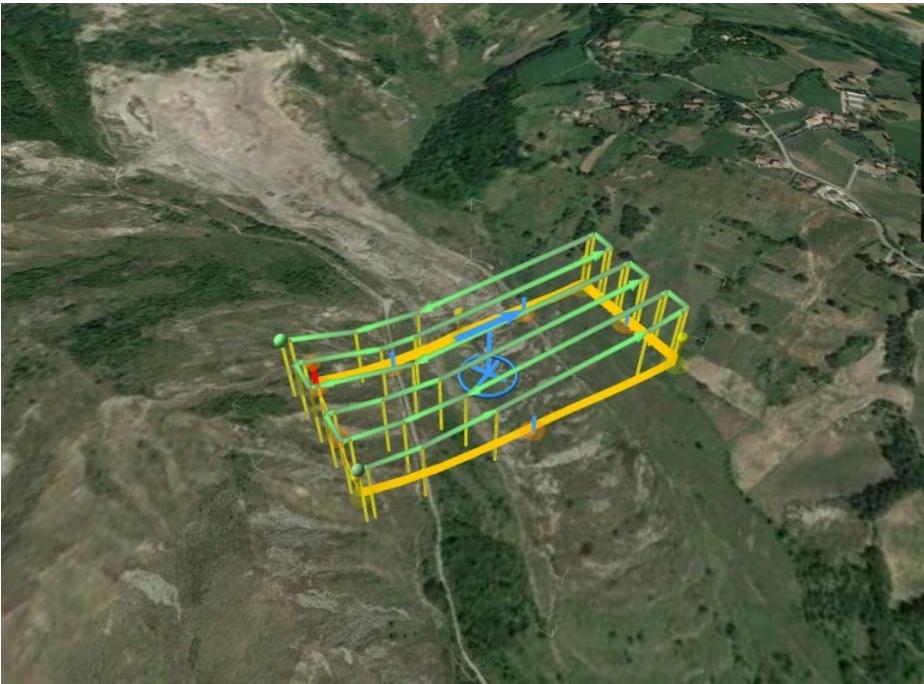
Figure 4. The flight plan of October 2020 on the Colata area.

Table 3. Flight specifications.

FLIGHTS			
Characteristics	October 2020 - Colata	April 2021 - Colata	April 2021 - Whole Area
GSD	1.00 cm	1.00 cm	1.00 cm
Flight speed	1.50 m/s	1.50 m/s	1.50 m/s
Forward overlap	60%	60%	60%
Side overlap	80%	80%	80%
Camera tilt	90° - 60°	90° - 60°	90°
F-Stop	F/2.8	F/2.8	F/2.8
Focal Lenght	8.8mm	35mm	35mm
Number of shoots	1413	2951	4762

For the survey performed in April 2021, three (**Error! Reference source not found.**) different flight missions were carried out. Several sub-missions have composed each mission to change batteries and download pictures from aircraft to storage.

Figure 5. Flightplans of the landslide's top part (left), median part (centre), the bottom part (foot).

2.1.3. Ground targets (GCPs-CkPs) and GNSS observations.

GNSS surveys have been carried out, in October 2020 and April 2021, for targets georeferencing and to switch from a relative frame to an absolute reference system. 36 ground targets (Figure 6) were installed on the study area, through deep-rooted poles (Figure 6), as reference points for photogrammetric reconstruction. They were also used to materialise a long-lasting reference for multitemporal GNSS monitoring. Some permanent GNSS stations, working for more than 6 years in the study area, have been physically linked to some ground targets. This rigid junction allows for having an accurate long-lasting ground truth. Each target was measured with the RTK mode and Network Real-Time Kinematic (NRTK), namely through Italpos service by Leica Geosystems (leica-geosystems.com). The receiver is an EMLID REACH RS2 multifrequency; the base receiver is an ItalPos service virtual base. In the second survey, in April 2021, the drone has an integrated RTK system, and a pseudo-direct survey has been carried out with the ItalPos virtual base service. The target position has been cquired with an EMLID REACH RS+ coupled with a permanent local base to obtain greater accuracy, Table 4 compares the specifications of the two EMLID receivers.

Figure 6. – Targets on a supporting pole.

Figure 7. Deep-rooted poles support ground targets.

Table 4. Technical specs of GNSS receivers.

POSITIONING		
Characteristics	**EMLID REACH RS+**	EMLID REACH RS2
Static horizontal	5.00 mm	4.00 mm + 0.5 ppm
Static vertical	10.00 mm	8 .00 mm + 1 ppm
Cinematic horizontal	7.00 mm	7.00 mm + 1 ppm
Cinematic vertical	14.00 mm	14.00 mm + 1 ppm
GNSS		
Signal	GPS/QZSS L1, GLONASS G1, BeiDou B1, Galileo E1,	GPS/QZSS L1C/A, L2C, GLONASS L1 OF, L2OF – BeiDou B1l, B2l, Galileo E1-B/c, E5b-SBAS L1C/A
Traced channels	72	184

2.2. UAS Image Processing

In this work, the software Agisoft Metashape 1.6.5 version has been used to process images acquired by UAS. The study area has been considered composed of a whole area

(
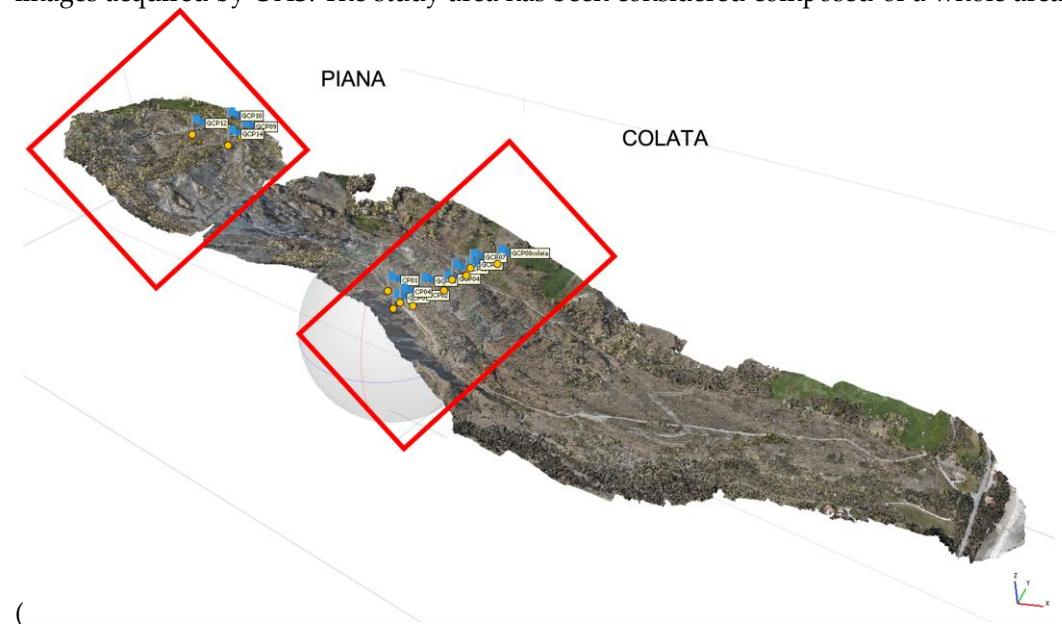
), the upper part, the so-called "Piana" (

) and the central part, so-called "Colata" (**Error! Reference source not found.**). For each area, a photogrammetric project has been created. The surveys have been performed in April 2021, and in October 2020, each area has two projects, apart from the whole area surveyed during the April 2021 campaign only. For each project, the images have been imported without camera specifications and have been filtered following a quality threshold as the first step. The software then estimated interior and exterior parameters using EXIF georeferencing information. GCPs and CkPs were measured and manually selected on the project images as a second step. For the whole area, Colata and Piana, 36 targets were selected. In particular, 12 CkPs and 24 GCPs. The GCPs were then selected as a constraint during the bundle block adjustment (BBA) procedure to put the photogrammetric reconstruction within a local coordinate system. CkPs was only selected as Control points. In order to easily integrate the performed survey with other technical maps, the European Terrestrial Reference System ETRS89 in planar representation TM32 on the Terrestrial Reference Frame ETFR200 has been chosen. Once the bundle adjustment processes had been performed, exterior and interior camera parameters were adjusted accurately. A comparison between GCPs and CkPs model coordinates and the coordinates observed by the GNSS survey has been performed to assess georeferencing process accuracy. The accuracy has been expressed in pixels and meters. Root mean square error has been calculated for the GCPs and CkPs better to depict the error distribution in the overall study area. GCPs and CkPs have been installed in the Piana and the Colata only.
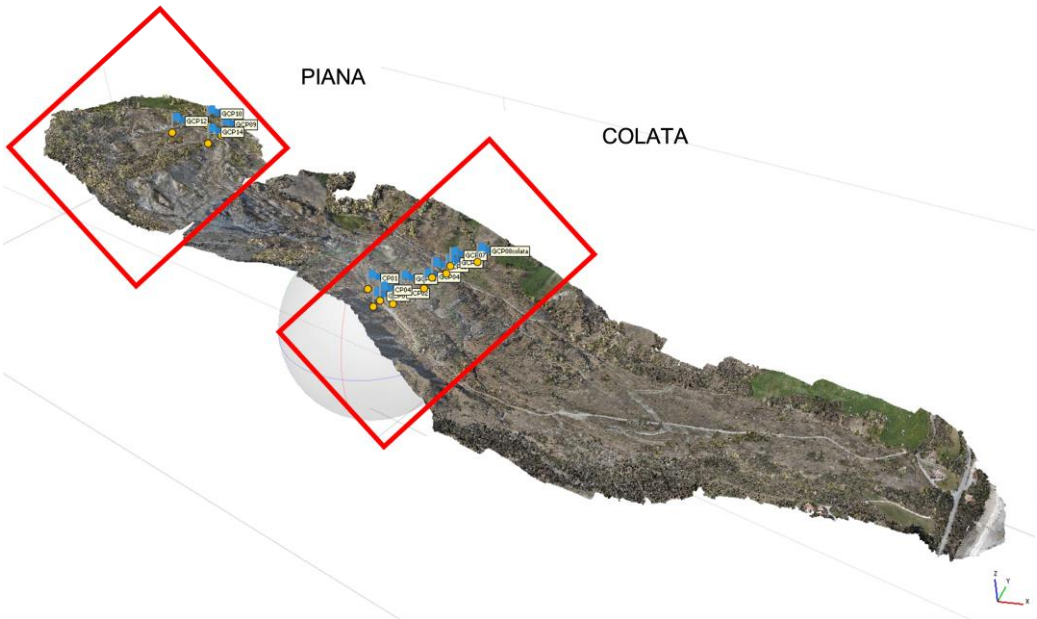
Figure 8. Dense point cloud of the whole landslide area.

Figure 9. Dense point cloud of the upper part of the Study area (Piana).

Figure 10. Dense point Cloud of the central part of the study area (Colata). The numbered flags on the ground surface represent the ground control points used for the bundle adjustment process.
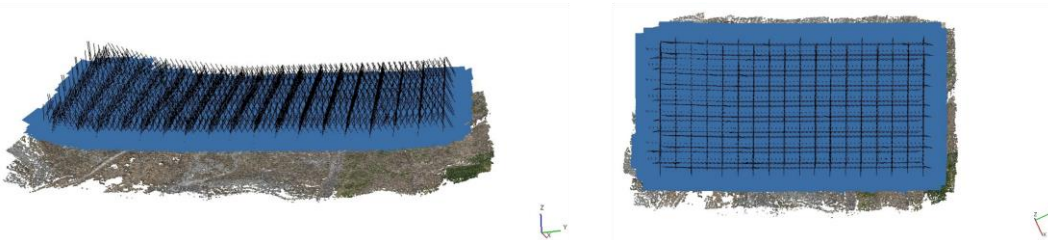
Figure 11. Prospect view (left) and top view (right) of the sparse point cloud of the Colata area during the April 2021 survey. The blue squares over the landslide show the camera positions and orientations during image acquisition by the UAS.

2.3. Digital Image Correlation (DIC)

DIC is an optical-numerical technique to quantify surface displacement. These deformations are calculated by comparing coregistered digital images collected at different epochs (Pan et al., 2008).

The correlation step in this process is essential and is based on searching for the maximum (or minimum) degree of correlation between the intensities within a reference region called the reference window (Pan et al., 2008). It is crucial to choose a suitable window's size; if it is too small, it will increase the noise of the image; instead, if it is too large, it may lose important details.

For this research, was used IRIS software owned by NHAZCA S.r.l. (Nhazca.it). The software wants as input a raster, and it was employed two orthomosaics with a resolution of 5 cm/px related to October 2020 and April 2021 derived from photogrammetric processing. In IRIS, performing pre-processing operations to standardise the images (called Master and Slave) and facilitate the detection of the movement is possible. After pre-processing, a Displacement Analysis with Phase Correlation (PC) algorithm was applied. The PC considers only the phase information but not the image content and base its functioning on the translation property of Fourier transform (FT). FT enunciate that "a shift of two relevant images in the spatial domain is transformed into the frequency domain as phase differences" [42]. The correlation function of Phase Correlation can be expressed through the inverse Fourier Transform of the normalised cross-power spectrum matrix Q:

$$\text{PC= F-1 } (Q(u, v) = \text{F-1 } \left\{ \frac{F(u,v)*G(u,v)}{|F(u,v)*G(u,v)|} \right\} = \text{F-1 } \{\exp (-i(u\Delta x + u\Delta y))\} \quad (1)$$

In formula (1) F(u, v) and G(u, v) are FT of f(x, y) and g(x, y) (the functions of two images), F-1 is the inverse FT, i = $\sqrt{-1}$,   Δx and Δy represent the shifts along with the two directions [41].

The PC method allows easy identification of the correlation peak given that the inverses FT of the normalised cross-power spectrum matrix Q is equivalent to Diarc delta function (formula 2) [41], [43].

PC = F-1 (Q(u, v) = F-1 {exp (-i(uΔx + uΔy))} = δ(x-Δx, y-Δy)   (2)

Some spatial filters have been applied at the end of the process to decrease the noise and improve visualisation. In figure 6 it is shown the result of the DIC process.
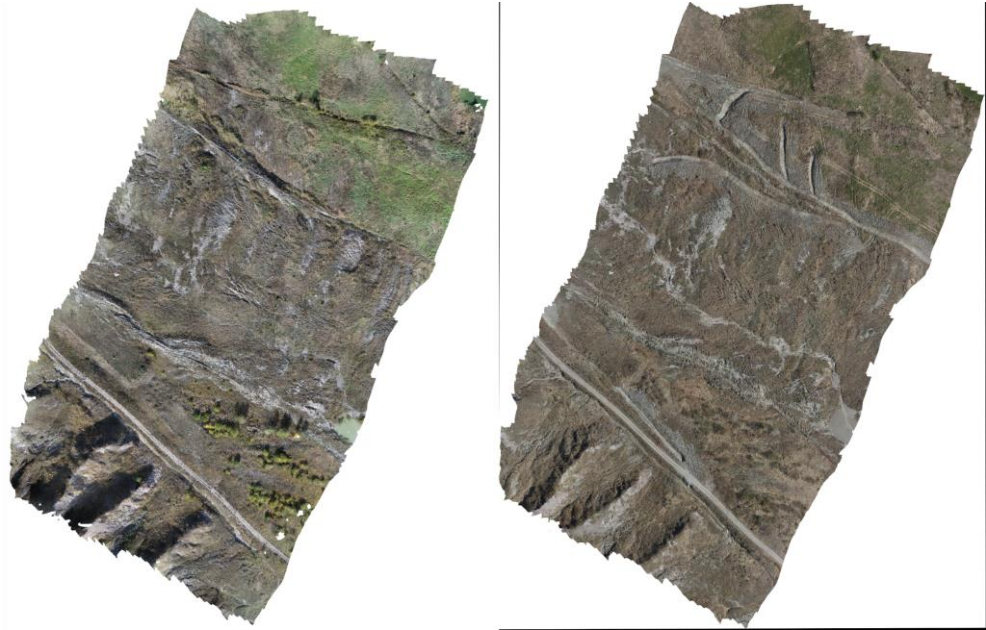
Figure 12. Ortomosaics were used to perform the DIC analysis. October 2020 (Left), April 2021 (Right).

The displacement values of DIC processing were compared with the targets' position to evaluate the analysis results (Ground Control Point, GCP) in the two epochs considered, April 2020 and October 2021 (**Error! Reference source not found.**).

3. Results

Results from the photogrammetric project analysis are presented, particularly Colata, end the whole landslide area have been considered individually. Digital Image Correlation analyses and comparison with GNSS monitoring campaigns are reported for the Colata area.

3.1. Photogrammetric Reconstruction

Considering surface irregularities spread all over the study area, each flight mission has been performed using nadiral and crossed (+ 60°, - 60°) views to optimise camera calibration and minimise shadowed areas. On the "whole area", the nadiral view only has been used to minimise the acquisition time. In table **Error! Reference source not found.**, RMSE for each of the performed projects is reported. As far as method B for the whole area region is concerned, the vast extension of the study area, the consistent presence of vegetation put several issues to the SfM software. The photogrammetric reconstruction did not succeed.

Table 5. RMS error summary table. Values are expressed in cm.

	RMS error X	RMS error Y	RMS error Z	RMS error Total
October 2020 – Colata – Method B				
GCP	1.73	2.21	0.88	2.94
CP	3.34	3.81	2.85	5.82
April 2021 – Colata – Method A				
GCP	-	-	-	-
CP	2.43	2.26	11.2	11.68
April 2021 – Colata – Method B				
GCP	0.79	0.94	1.41	1.87
CP	1.32	1.09	3.12	3.56
April 2021 – Colata – Method C				
GCP	1.27	0.80	0.27	1.53
CP	2.52	3,95	2.06	5.00
April 2021 – whole area – Method A				
GCP	-	-	-	-
CP	7.17	9.46	23.61	26.43
April 2021 – whole area– Method B				
GCP	-	-	-	-
CP	-	-	-	-
April 2021 – whole area – Method C				
GCP	2.56	2.58	0.99	3.77
CP	1.83	3.57	1.67	4.35

3.2. Digital Image Correlation

The main product from Digital Image Correlation is a deformation map (**Error! Reference source not found.**). The analysis has been carried out on the "Colata" in the landslide medium part. The deformation map shows a central part in which surface deformation is visible. In particular, the flow direction is oriented from the northwest to South-East.
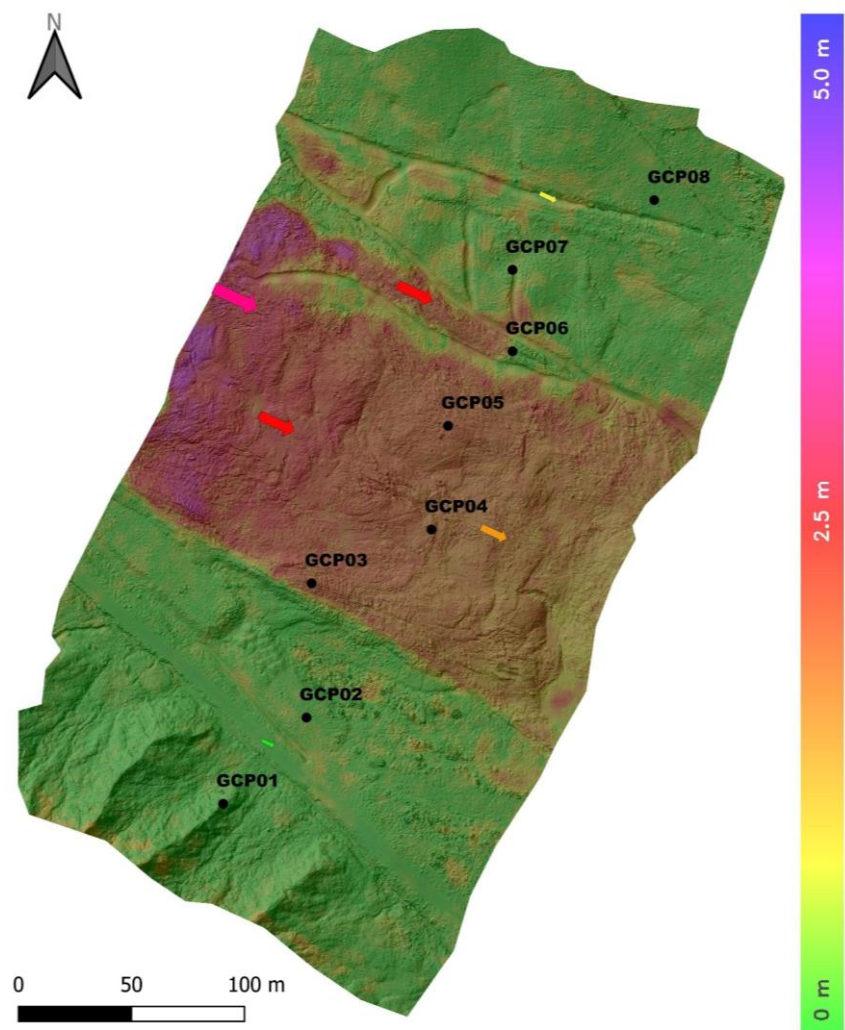
Figure 13. Deformation map from Digital Image Correlation.

The displacement values estimated with DIC processing were compared with the different positions of targets (Ground Control Point, GCP), measured with GNSS, in the two considered times. The comparison is shown in Table 6. **Error! Reference source not found.** shows GCPs positions observed in April 2021 (green) and October 2020 (pink). The mean square deviation is 0.077 m.
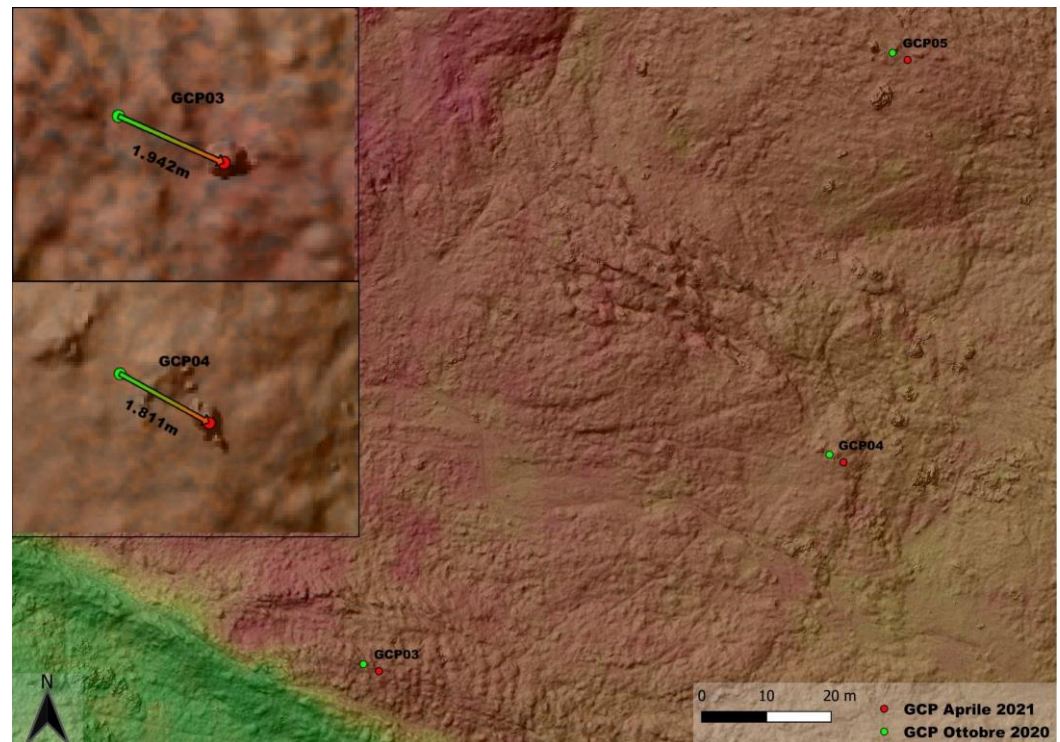
Figure 14. GCP positions were observed in April (green) and October (pink) on the colata area.

Table 6. Comparison GNSS survey results / DIC Analysis results.

GCP	GNSS movement	DIC movement	Deviation
GCP01	0.200 m	0.112 m	-0.088 m
GCP02	0.190 m	0.229 m	0.039 m
GCP03	1.942 m	1.879 m	-0.063 m
GCP04	1.811 m	1.789m	-0.022 m
GCP05	1.892 m	1.867 m	-0.025 m
GCP06	0.258 m	0.351 m	0.093 m
GCP07	0.207 m	0.351 m	0.168 m
GCP08	0.013 m	0.206 m	0.193 m

4. Discussion

In this study, the integration of photogrammetric surveys with GNSS permanent local monitoring allowed for investigating the effectiveness of photogrammetry as a tool for monitoring land deformations in complicated, vast and risk-prone areas. Direct and indirect georeferencing play a crucial role in determining the survey's accuracy. The whole studying area, of about 0.9 Km2, is also covered by vegetation, mostly grass from 10 to 60 cm tall (70%), some rushes area (2%) from 0,5 to 1,5 meters tall, and very sporadic areas with tall vegetation (< 0,3%).

In such a context, deploying a reliable and robust monitoring system could be a costly initiative, both in terms o time and money. Furthermore, maintaining a complex monitoring system as a RADAR SAR or multiple Total Station networks could be too demanding for small administrations like local municipalities. In this framework, the integration of detailed photogrammetric surveys, GNSS monitoring and Digital Image Correlation analyses have been exploited to investigate performances of a monitoring system based on ortophotomosaics from UAS photogrammetric campaigns.

Looking at the survey accuracy from photogrammetric reconstruction, comparing results from the April 2021 campaign carried out with Matrice 300 with P1 camera configuration, a lower RMSE is achieved with the indirect georeferencing procedure. The

obtained value of 3 cm is almost one order of magnitude lower than that obtained through direct georeferencing, 24,4 cm.

By analysing results, an unexpected result needs to be interpreted. In particular, the C method should bring to best performances in terms of accuracy. On the contrary, as reported in Table 7, the photogrammetric reconstruction showed a better accuracy using method B. Theoretically, a more significant number of references should bring to a most accurate reconstruction. Georeferencing procedure for the C method is made with an in-field survey only; on the contrary, the B method merges the in-field GNSS survey with the onboard GNSS RTK observations. However, in this case, despite the onboard GNSS having brought some more information to be digested by the SfM software, the final result does not comply with the expectation of finding better accuracy.

Table 7. Comparison Method B and Method C. RMSE values are expressed in cm.

Survey April 2021 – Colata – Method B	
GCP	1.87
CP	3.56
Survey April 2021 – Colata – Method C	
GCP	1.53
CP	**5**

The difference of about 1.5 cm could also be credited to the different base stations used for the GNSS in-field survey and onboard. For the B method, a GNSS permanent local station has been used. The permanent GNSS local station is a single frequency, and the onboard GNSS receiver is double frequency; using the permanent local base as RTK base for the onboard UAS receiver has not been possible. The cause of this unexpected result is most likely to be addressed to the hi-precision but low accuracy that virtual GNSS NRTK stations often guarantee. According to [44]) landslide can be classified in terms of velocity.

Table 8. Landslide velocity classification.

Velocity class	Description	Velocity (mm/s)	Typical velocity	Response[a]
7	Extremely rapid	$5{\times}10^{3}$	5 m/s	Nil
6	Very rapid	$5{\times}10^{1}$	3 m/min	Nil
5	Rapid	$5{\times}10^{-1}$	1.8 m/h	Evacuation
4	Moderate	$5{\times}10^{-3}$	13 m/month	Evacuation
3	Slow	$5{\times}10^{-5}$	1.6 m/year	Maintenance
2	Very slow	$5{\times}10^{-7}$	16 mm/year	Maintenance
1	Extremely slow			Nil

From historical and recent monitoring activities [34], [45]), the deformative process on the study area could be considered a slow to moderate velocity, classes 3-4. Applying the "A" method, which allows for 24 cm of accuracy, allows for effective monitoring performances on the whole area, guaranteeing a minimum time recurrency from 1 to 6 months; measuring a 50 cm displacement is plausible with an accuracy of 24 cm.

In the "colata" area, where 8 aligned targets were installed, the A, B and C methods also allow for adequate monitoring performances. Especially for the B case, with an accuracy of less than 4 cm, it allows for a minimum time recurrency up to some hours in case of a moderate deformation velocity.

5. Conclusions

The presented paper investigated how a photogrammetric campaign can perform deformation monitoring on a landslide body in a real case study. On a large landslide with

compound deformative processes, 36 permanent ground targets have been installed through deep-rooted poles. Considering the considerable size of the landslide area, which is 0.9 Km2, deploying Ground Targets (GCPs and CkPs) with optimum geometrical distribution to achieve a proper photogrammetric survey is a very tough task. Furthermore, the area is strewn with marshy areas and a diffuse presence of hi-risk zones with collapsing material and unstable gullies. A considerable amount of investments should be provided to set up a proper photogrammetric survey with an optimised GCPs network in such a landslide area. This study shows that even with a few GCPs, integrating photogrammetric survey, Digital Image Correlation analysis, and GNSS monitoring can achieve effective deformation monitoring by applying indirect georeferencing. With a worse overall accuracy (0.24 m), pseudo-direct georeferencing may also produce sound indications on the deformation pattern. GNSS permanent stations give reliable, long-lasting knowledge on local deformation speed. Photogrammetry allows extending to the overall area GNSS observations with a valuable consistency. Finally, Digital Image Correlation analysis allows a detailed deformation map, a proper tool for interpreting deformations and landslide dynamics.

Author Contributions: Conceptualization, Francesco Mugnai; Data curation, Francesco Mugnai; Formal analysis, Francesco Mugnai; Investigation, Francesco Mugnai; Methodology, Francesco Mugnai; Resources, Andrea Masiero; Software, Francesco Mugnai; Supervision, Francesco Mugnai, Andrea Masiero; Validation, Francesco Mugnai; Visualization, Francesco Mugnai; Writing – original draft, Francesco Mugnai; Writing – review & editing, Francesco Mugnai.

Funding: This research received no external funding

Data Availability Statement: Data is available on request from the authors. The data supporting this study's findings are available from the corresponding author, [Mugnai F.], upon reasonable request.

Acknowledgments: The authors would like to thank Dr. Giovanni Bertolini, Regione Emilia-Romagna - Agenzia per la Sicurezza Territoriale e Protezione Civile Servizio Sicurezza Territoriale e Protezione Civile di Reggio Emilia, Via Emilia Santo Stefano 25, 42100 Reggio Emilia; Prof. Alessandro Corsini, Dr. Marco Mulas, Dr. Giuseppe Ciccarese; Department of Chemical and Geological Sciences, Via Università 4, 41121 Modena; Dr. Riccardo Angelini, Dr. Irene Cortesi, Prof. Grazia Tucci, Department of Civil and Environmental Engineering, University of Florence, via di S.Marta, 3 - 50139 Firenze, Italy;

Conflicts of Interest: The authors declare no conflict of interest

References

1. P. Sestras, Ștefan Bilașco, S. Roșca, B. Dudic, A. Hysa, and V. Spalević, "Geodetic and UAV Monitoring in the Sustainable Management of Shallow Landslides and Erosion of a Susceptible Urban Environment," Remote Sens., vol. 13, no. 3, p. 385, 2021.
2. D. Turner, A. Lucieer, and S. M. de Jong, "Time series analysis of landslide dynamics using an Unmanned Aerial Vehicle (UAV)," Remote Sens., vol. 7, no. 2, pp. 1736–1757, 2015, doi: 10.3390/rs70201736.
3. R. Cefalo et al., "'Paleo-environmental Researches on Aquileia territory in the ancient times' View project Integrated Topographic, GNSS, Remote Sensing and GIS/WebGIS Techniques Applied to the Study of Aquileia River Port Structures," 2011. Accessed: Jun. 22, 2021. [Online]. Available: https://www.researchgate.net/publication/221333492.
4. G. Lindner, K. Schraml, R. Mansberger, and J. Hübl, "UAV monitoring and documentation of a large landslide," Appl. Geomatics, vol. 8, no. 1, pp. 1–11, 2016.
5. D. Leva, G. Nico, D. Tarchi, J. Fortuny-Guasch, and A. J. Sieber, "Temporal analysis of a landslide by means of a ground-based SAR interferometer," IEEE Trans. Geosci. Remote Sens., vol. 41, no. 4, pp. 745–752, 2003.
6. G. Luzi et al., "Ground-based radar interferometry for landslides monitoring: atmospheric and instrumental decorrelation sources on experimental data," IEEE Trans. Geosci. Remote Sens., vol. 42, no. 11, pp. 2454–2466, 2004.
7. Turrisi Simone, "Motion blur compensation to improve the accuracy of Digital Image Correlation measurements." Politecnico di Milano, 2017.
8. M. Lazecký, F. C. Çomut, I. Hlaváčová, and Ş. Gürboğa, "Practical application of satellite-based SAR interferometry for the detection of landslide activity," Procedia Earth Planet. Sci., vol. 15, pp. 613–618, 2015.
9. M. Pieraccini and L. Miccinesi, "Ground-based radar interferometry: A bibliographic review," Remote Sens., vol. 11, no. 9, p. 1029, 2019.
10. J. Wasowski and F. Bovenga, "Remote sensing of landslide motion with emphasis on satellite multi-temporal interferometry applications: an overview," Landslide Hazards, Risks, and Disasters, pp. 365–438, 2022.

11. D. Notti, J. C. Davalillo, G. Herrera, and O. Mora, "Assessment of the performance of X-band satellite radar data for land-slide mapping and monitoring: Upper Tena Valley case study," Nat. Hazards Earth Syst. Sci., vol. 10, no. 9, pp. 1865–1875, 2010.

12. G. B. Crosta, F. Agliardi, C. Rivolta, S. Alberti, and L. Dei Cas, "Long-term evolution and early warning strategies for complex rockslides by real-time monitoring," Landslides, vol. 14, no. 5, pp. 1615–1632, 2017.

13. F. Bellotti, M. Bianchi, D. Colombo, A. Ferretti, and A. Tamburini, "Advanced InSAR techniques to support landslide monitoring," in Mathematics of planet earth, Springer, 2014, pp. 287–290.

14. G. Antonello et al., "Microwave interferometric sensors as a tool for space and time analysis of active volcano deformations: The Stromboli case," in Use of Remote Sensing Techniques for Monitoring Volcanoes and Seismogenic Areas, 2008. USEReST 2008. Second Workshop on, 2008, pp. 1–6.

15. T. Strozzi, R. Delaloye, A. Kääb, C. Ambrosi, E. Perruchoud, and U. Wegmüller, "Combined observations of rock mass movements using satellite SAR interferometry, differential GPS, airborne digital photogrammetry, and airborne photography interpretation," J. Geophys. Res. Earth Surf., vol. 115, no. F1, 2010.

16. Z. Xiong et al., "Pre-and post-failure spatial-temporal deformation pattern of the Baige landslide retrieved from multiple radar and optical satellite images," Eng. Geol., vol. 279, p. 105880, 2020.

17. L. Mucchi et al., "A flexible wireless sensor network based on ultra-wide band technology for ground instability monitoring," Sensors, vol. 18, no. 9, p. 2948, 2018.

18. M. M. Nicotra, R. Naldi, and E. Garone, "Nonlinear control of a tethered UAV: The taut cable case," Automatica, vol. 78, pp. 174–184, 2017.

19. X. Xiao, J. Dufek, and R. Murphy, "Benchmarking tether-based uav motion primitives," in 2019 IEEE International Symposium on Safety, Security, and Rescue Robotics (SSRR), 2019, pp. 51–55.

20. O. Hungr, S. Leroueil, and L. Picarelli, "The Varnes classification of landslide types, an update," Landslides, vol. 11, no. 2, pp. 167–194, 2014.

21. G. Blasone, M. Cavalli, L. Marchi, and F. Cazorzi, "Monitoring sediment source areas in a debris-flow catchment using terrestrial laser scanning," Catena, vol. 123, pp. 23–36, 2014.

22. D. J. Milan, G. L. Heritage, A. R. G. Large, and I. C. Fuller, "Filtering spatial error from DEMs: Implications for morphological change estimation," Geomorphology, vol. 125, no. 1, pp. 160–171, 2011.

23. Y. Taddia, C. Corbau, E. Zambello, and A. Pellegrinelli, "UAVs for structure-from-motion coastal monitoring: a case study to assess the evolution of embryo dunes over a two-year time frame in the Po River Delta, Italy," Sensors, vol. 19, no. 7, p. 1717, 2019.

24. N. McCormick and J. Lord, "Digital image correlation," Mater. today, vol. 13, no. 12, pp. 52–54, 2010.

25. M. A. Sutton et al., "Recent progress in digital image correlation: background and developments since the 2013 WM Murray Lecture," Exp. Mech., vol. 57, no. 1, pp. 1–30, 2017.

26. B. Pan, "Digital image correlation for surface deformation measurement: historical developments, recent advances and future goals," Meas. Sci. Technol., vol. 29, no. 8, p. 82001, 2018.

27. M. Quanjin, M. R. M. Rejab, Q. Halim, M. N. M. Merzuki, and M. A. H. Darus, "Experimental investigation of the tensile test using digital image correlation (DIC) method," Mater. Today Proc., vol. 27, pp. 757–763, 2020.

28. F. Mugnai, G. Tucci, and A. Da Re, "DIGITAL IMAGE CORRELATION IN ASSESSING STRUCTURED-LIGHT 3D SCANNER'S GANTRY STABILITY: PERFORMING DAVID'S (MICHELANGELO) HIGH-ACCURACY 3D SURVEY," Int. Arch. Photogramm. Remote Sens. Spat. Inf. Sci., vol. XLVI-M-1–2, pp. 463–469, Aug. 2021, doi: 10.5194/isprs-archives-XLVI-M-1-2021-463-2021.

29. Z. Chen and S. H. Daly, "Active slip system identification in polycrystalline metals by digital image correlation (DIC)," Exp. Mech., vol. 57, no. 1, pp. 115–127, 2017.

30. P. Caporossi, P. Mazzanti, and F. Bozzano, "Digital image correlation (DIC) analysis of the 3 December 2013 Montescaglioso landslide (Basilicata, southern Italy): results from a multi-dataset investigation," ISPRS Int. J. Geo-Information, vol. 7, no. 9, p. 372, 2018.

31. T. C. Chu, W. F. Ranson, and M. A. Sutton, "Applications of digital-image-correlation techniques to experimental mechanics," Exp. Mech., vol. 25, no. 3, pp. 232–244, 1985.

32. S. Yoneyama and G. Murasawa, "Digital image correlation," Exp. Mech., vol. 207, 2009.

33. J. Zhao, Y. Sang, and F. Duan, "The state of the art of two-dimensional digital image correlation computational method," Eng. Reports, vol. 1, no. 2, p. e12038, 2019.

34. M. Mulas, G. Ciccarese, G. Truffelli, and A. Corsini, "Integration of digital image correlation of sentinel-2 data and continuous gnss for long-term slope movements monitoring in moderately rapid landslides," Remote Sens., vol. 12, no. 16, pp. 1–17, 2020, doi: 10.3390/RS12162605.

35. A. Lucieer, S. M. de Jong, and D. Turner, "Mapping landslide displacements using Structure from Motion (SfM) and image correlation of multi-temporal UAV photography," Prog. Phys. Geogr., vol. 38, no. 1, pp. 97–116, 2014.

36. B. Shi and C. Liu, "UAV for landslide mapping and deformation analysis," in International Conference on Intelligent Earth Observing and Applications 2015, 2015, vol. 9808, p. 98080P.

37. E. Puniach, W. Gruszczyński, P. Ćwiąkała, and W. Matwij, "Application of UAV-based orthomosaics for determination of horizontal displacement caused by underground mining," ISPRS J. Photogramm. Remote Sens., vol. 174, pp. 282–303, Apr. 2021, doi: 10.1016/j.isprsjprs.2021.02.006.

38. F. Cervi, F. Ronchetti, G. Martinelli, T. A. Bogaard, and A. Corsini, "Origin and assessment of deep groundwater inflow in the Ca' Lita landslide using hydrochemistry and in situ monitoring," Hydrol. Earth Syst. Sci., vol. 16, no. 11, pp. 4205–4221, 2012, doi: 10.5194/hess-16-4205-2012.

39. M. Mulas, G. Ciccarese, G. Truffelli, and A. Corsini, "Displacements of an active moderately rapid landslide—A dataset retrieved by continuous gnss arrays," Data, vol. 5, no. 3, pp. 1–6, 2020, doi: 10.3390/data5030071.

40. L. Borgatti et al., "Large reactivated landslides in weak rock masses: A case study from the Northern Apennines (Italy)," Landslides, vol. 3, no. 2, pp. 115–124, 2006, doi: 10.1007/s10346-005-0033-9.

41. B. Pan, H. Xie, Z. Wang, K. Qian, and Z. Wang, "Study on subset size selection in digital image correlation for speckle patterns," Opt. Express, vol. 16, no. 10, pp. 7037–7048, 2008.

42. X. Tong et al., "Image Registration with Fourier-Based Image Correlation: A Comprehensive Review of Developments and Applications," IEEE J. Sel. Top. Appl. Earth Obs. Remote Sens., vol. 12, no. 10, pp. 4062–4081, 2019, doi: 10.1109/JSTARS.2019.2937690.

43. V. Balakrishnan, "All about the Dirac delta function (?)," Resonance, vol. 8, no. 8, pp. 48–58, 2003.

44. D. M. Cruden and D. J. Varnes, "Cruden, DM, Varnes, DJ, 1996, Landslide Types and Processes, Transportation Research Board, US National Academy of Sciences, Special Report, 247: 36-75," Landslides Eng. Pract., vol. 24, pp. 20–47, 1993.

45. A. Rosi et al., "Environmental Monitoring and Task-Driven Computing," IEEE Pervasive Comput., vol. 9, no. 4, pp. 48–50, 2010.